Simultaneous Radar and Communication Emissions from a Common Aperture, Part II: Experimentation

Patrick M. McCormick,
Brandon Ravenscroft,
and Shannon D. Blunt
Radar Systems Lab
University of Kansas
Lawrence, KS

Andrew J. Duly
and Justin G. Metcalf
Sensors Directorate
Air Force Research Lab
Wright-Patterson AFB, OH

***Abstract*—In the companion paper the Far-Field Radiated Emission Design (FFRED) formulation was theoretically derived for the application of simultaneous generation of multi-function radar and communication emissions in the same spectrum from the same antenna array via a physically realizable MIMO transmit arrangement. Here the practical consequences of such a transmission scheme are considered by way of experimental measurements. The multi-function waveforms were implemented on an Air Force Research Laboratory (AFRL) software-defined radar testbed comprised of four independent transmit channels. Experimental results from a compact range include beampattern measurements, radar waveform validation, and bit error rate analysis of the communication beam.**

***Index Terms*—multi-function RF, spectrum sharing, MIMO radar, communications**

I. Introduction

As antenna array technology progresses, sophisticated emission schemes and signal processing methods that were previously infeasible begin to become possible. Specifically, a fully digital array represents a leap in technological capability over traditional active electronically steered arrays (AESAs). In contrast to an AESA, a fully digital array possesses an independent transmit and receive channel behind each element (or sub-array), thereby permitting independent waveform generation at each element. The versatility of these arrays facilitates the realization of multiple functions on the same system. For example, the Advanced Multi-Function RF Concept (AMRFC) [1] employed a flexible sub-arraying capability to share different transmit modes simultaneously. Taking this notion even further, here we consider the practical requirements and experiment validation of the emission scheme developed in the companion paper [2] in which both radar and communication signals are realized in the far-field via a multiple-input multiple-output (MIMO) combination of all transmitted signals.

In recent years various instantiations of the MIMO radar concept have emerged. A specific example is that of correlated MIMO, in which the set of waveforms are correlated so as to enable the formation of multiple beams in separate directions (e.g. [3], [4]). Previous work has also examined ways in which to design waveforms that produce a desired far-field beampattern (e.g. [4]–[7]), albeit without controlling the fast-time structure of the far-field signals. In [3] the beampattern is determined analytically, though the waveforms are not guaranteed to meet the requirements for physical generation by a high-power radar transmitter (see [8]).

In the companion paper [2], a form of correlated MIMO was theoretically developed that enables control of the far-field time domain signals that are emitted in particular spatial directions. Moreover, the multi-function waveforms designed to generate this effect all have constant amplitude and are well contained spectrally so as to be amenable to a high-power amplifier (HPA) [8]. This design approach is denoted as far-field radiated emission design (FFRED) and combines a minimum norm solution for the (over-sampled) discretized waveform matrix with a supplemental matrix that provides the additional degrees of freedom necessary to maintain constant amplitude. The resulting FFRED approach is a form of alternating projections [9]–[12] that trades an increase in spatial sidelobes [2] for physically realizable waveforms that are implementable in a high-power radar system. Here we establish the efficacy of this approach by experimentally demonstrating a simultaneous dual radar/communication emission using the BEEMER software-defined radar testbed at AFRL [13].

II. Practical Considerations for Far-Field Radiated Emission Design (FFRED)

The FFRED formulation involves an iterative process to solve a pair of optimization problems possessing an error reduction property to produce a set of optimized, constant amplitude waveforms that are amenable for transmission by a high-power radar. The desired far-field emissions are illustrated in Fig. 1.

While the desired radar signal $g_{\rm r}(t)$ and communication signal $g_{\rm c}(t)$ can be readily designed for direct implementation, the determination of a set of physically realizable waveforms that could generate these signals via constructive/destructive combining in the far-field is more complicated. The FFRED solution from [2] determines the minimum-norm estimate of this set of waveforms to produce $g_{\rm r}(t)$ and $g_{\rm c}(t)$, and then uses an orthogonal subspace to "top off" these minimum-norm

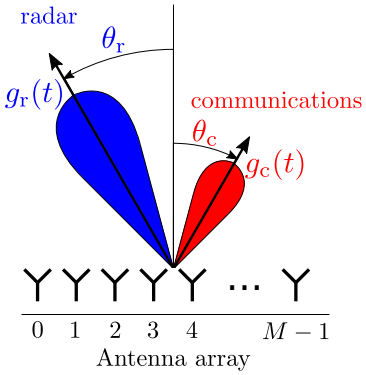

Fig. 1. Simultaneous emission of radar and communication signals from a common antenna array

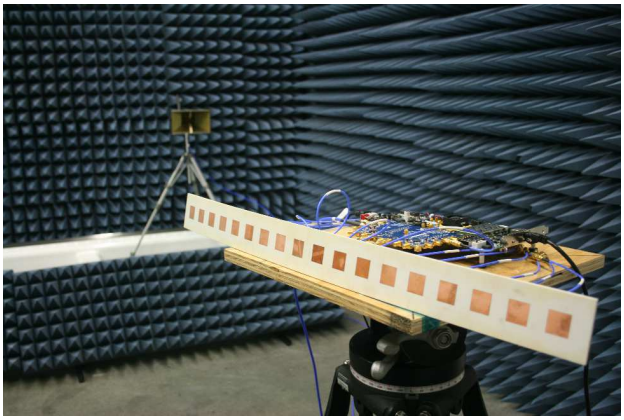

Fig. 2. Experimental setup: BEEMER and array in foreground, and receive horn antenna in background.

estimates to enforce constant amplitude. Further, by "over-sampling" the waveforms in the time-domain (with respect to 3 dB bandwidth) sufficient spectral containment is maintained to ensure the waveforms are physically amenable to the transmitter.

To maintain this physical compliance, FFRED removes a fraction of the power from the radar and communication beams and places it in orthogonal complement spatial directions. However, the power efficiency gained by using transmitter-amenable waveforms compensates for this "wasted" power. Another key aspect is that while $g_r(t)$ and $g_c(t)$ are required to occupy the same pulse length and bandwidth, they are otherwise unconstrained, thus the structure of the communication signal and radar waveform can be changed as needed.

One parameter that FFRED requires is the percentage of power to allocate to the orthogonal complement subspace. It is shown in [2] that increasing the amount of power in this subspace improves convergence behavior. The average power emitted by the digital array is

$$\gamma^2 = \rho_\star + \rho_\perp, \tag{1}$$

where $\rho_\perp$ is the power allocated to the orthogonal complement subspace and $\rho_\star$ is the power allocated to the radar and communication beams based on minimum-norm optimization [2]. The percent orthogonal power is then defined as

$$\%\rho_\perp = \frac{\rho_\perp}{\gamma^2} \times 100\%. \tag{2}$$

The impact of various values of $\%\rho_\perp$ is shown in [2].

III. Experimental Results

The FFRED-derived multi-function waveforms were experimentally validated through open air testing in an indoor facility at the AFRL Sensors Directorate. The BEEMER (Baseband-digital at Every Element MIMO Experimental Radar) software-defined radar (SDR) system [13] served as the RF and digital backend for the experiment. These experiments require hardware that provides independent, element-level waveform generation, a requirement met by the BEEMER SDR.

The aperture consisted of an 18 element linear patch array antenna with half-wavelength inter-element spacing at 3.5 GHz. Four transmit channels were connected to the centermost elements of the array to reduce edge effects on the element patterns. The emission was measured using one receive channel of the BEEMER system captured at 40 MS/s baseband I/Q connected to a quad-ridge horn with 18 dBi of gain. Fig. 2 shows the transmit array, BEEMER system, and horn antenna inside the chamber used to capture the signals, with the transmit and receive antennas separated by 3 m. Boresight calibration was initially performed to calibrate the amplitude and phase offsets across the four transmit channels of the SDR. Frequency-dependent calibration of the SDR was not performed as this would alter the constant amplitude structure of the waveforms.

The radar waveform is an up-chirped LFM with a bandwidth of 10 MHz and pulsewidth of 10 μs for a time-bandwidth product of 100. The communications beam is set to have 13 dB less power than the radar beam as the communication link is assumed to be secondary to the radar mission and would only have to contend with one-way path losses in practice. For these tests, the communication beam was pointed at $\theta_c = 30°$. Two different radar beam directions were considered at $\theta_r = -15°$ and $\theta_r = 0°$, such that the communication emission corresponds to the first sidelobe and first null of the radar emission, respectively. The steering vectors for the radar and communication beams were estimated prior to testing for use in the transmit model for waveform optimization (for more information see [2]).

The communication signals are modulated using a QPSK constellation with either a rectangular (RECT) filter, yielding 200 bits per pulse, or a square-root raised-cosine (SRRC) filter [14] that yields 180 bits per pulse. The latter provides better spectral containment but introduces a high of amplitude modulation that increases the average orthogonal power needed for convergence. Fig. 3 shows the spectrum of the radar waveform (blue) and the envelopes of the communication signals with RECT (red) and SRRC (yellow) shaping filters.

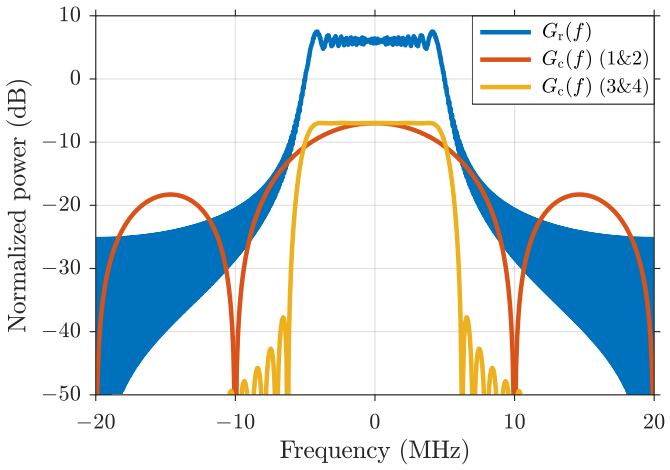

Fig. 3. Spectral content of radar waveform (blue) and QPSK modulated communications using a RECT filter (red) and SRRC filter (yellow).

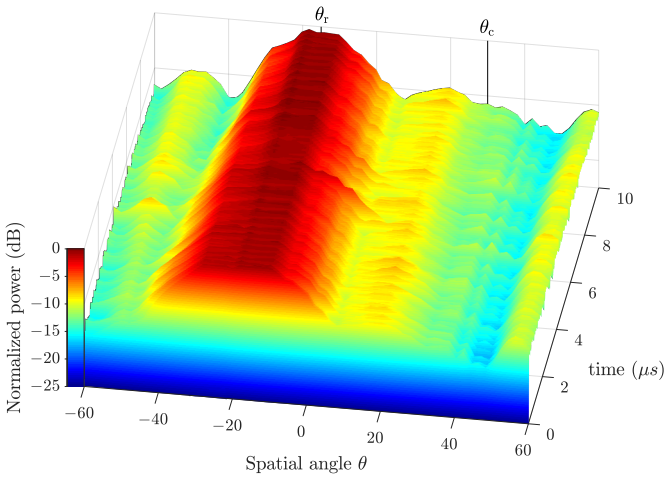

Fig. 4. Average emitted power versus spatial angle θ and fast-time for case 1 ($\theta_r = -15°$ and RECT shaping filter).

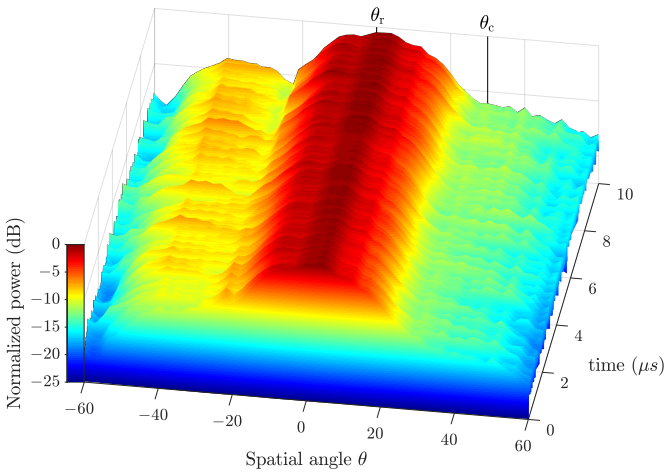

Fig. 5. Average emitted power versus spatial angle θ and fast-time for case 2 ($\theta_r = 0°$ and RECT shaping filter).

TABLE I
TEST CASE PARAMETERS

	Radar direction θ_r	**Shaping filter**
Case 1	$-15°$	RECT
Case 2	$0°$	RECT
Case 3	$-15°$	SRRC
Case 4	$0°$	SRRC

TABLE II
SUMMARY OF FIXED PARAMETERS

Parameter	**Value**
Center frequency	3.5 GHz
Bandwidth	10 MHz
Pulsewidth	10 μs
Active antenna elements	4
Antenna element spacing	8.57 cm (half-wavelength)
Receiver sampling rate	40 MS/s
Communication direction θ_c	$30°$
Relative comm power (dB)	-13 dB
Communications modulation	QPSK (gray-coded)
Radar modulation	Up-chirped LFM
Transmitted pulses	20
Bits transmitted per pulse	200 (RECT)
	180 (SRRC)

Table I summarizes the four test cases arising from the combination of two different modes of communication modulation and two different radar emission directions. Twenty pulses were transmitted for each test case resulting in a total of 4000 bits for cases 1 and 2, and 3600 bits for cases 3 and 4. While sample size is clearly not large enough to accurately predict the true bit-error rate, it is sufficient to demonstrate the validity of this manner of dual-function radar/communication.

The goals of these tests are to characterize how accurately the far-field signals could be produced in their corresponding desired directions and to assess the impact of the minimum percent orthogonal power for optimization. A summary of all other parameters is provided in Table II. These parameters and the steering vector estimates were then used inside the optimization procedure to generate the multi-function waveforms according to [2].

For cases 1 and 2 (RECT shaping filter) the average minimum percent orthogonal power to achieve convergence was $\%\rho_\perp = 16.19\%$. For cases 3 and 4 (SRRC shaping filter) the average minimum orthogonal power was $\%\rho_\perp = 30.25\%$. Thus the amplitude modulation induced by the SRRC shaping filter necessitates almost a doubling of the orthogonal power needed to converge. The different spatial separations between the radar and communication beams had a negligible impact on percent orthogonal power for this small number of antenna elements.

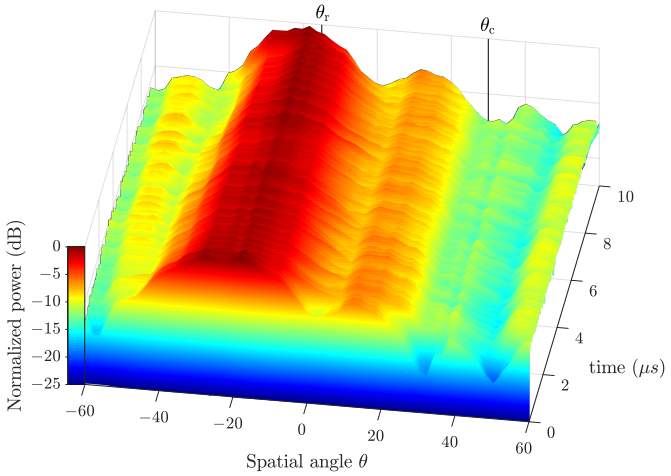

Fig. 6. Average emitted power versus spatial angle θ and fast-time for case 3 ($\theta_r = -15°$ and SRRC shaping filter).

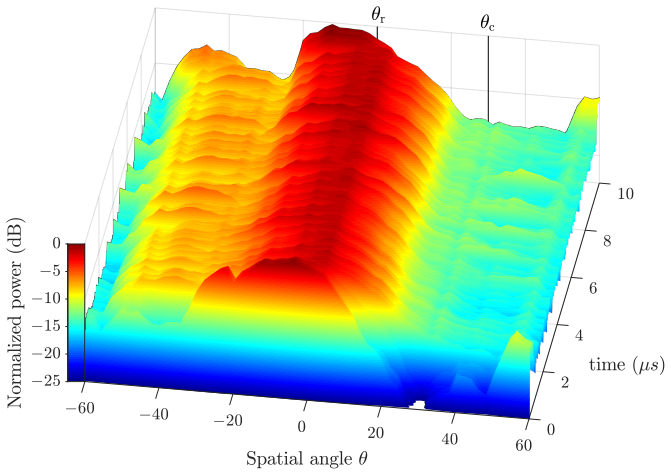

Fig. 7. Average emitted power versus spatial angle θ and fast-time for case 4 ($\theta_r = 0°$ and SRRC shaping filter).

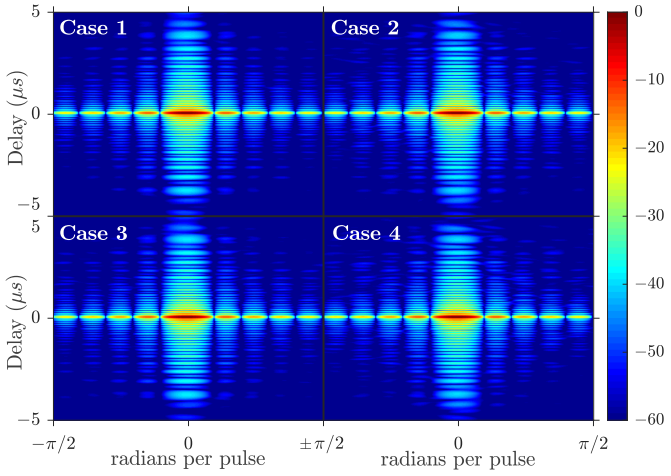

Fig. 8. Range-Doppler response for radar beam directions for the four cases.

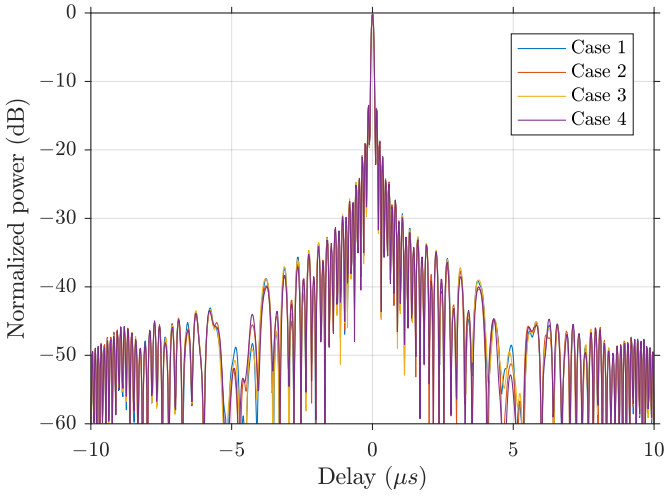

Fig. 9. Zero-Doppler cut for radar beam directions for case 1 (blue), case 2 (red), case 3 (yellow), and case 4 (purple).

The four sets of MIMO emissions were captured from $-60°$ to $60°$ at $2°$ increments. The average emitted power versus angle θ and fast-time are shown in Figs. 4 and 5 for cases 1 and 2, respectively. Note how additional transmit power is apparent in directions other than the radar and communication directions. This additional power corresponds to the percent orthogonal power needed to realize a set of constant amplitude waveforms. Also note that the placement of the energy is dependent on the orientation of the radar and communication beams, and for case 2 is symmetric to the actual communication direction.

The average emitted power versus θ and fast-time for cases 3 and 4 are shown in Figs. 6 and 7, respectively. The almost two-fold increase in percent orthogonal power for these cases is apparent as the additional power in other directions is noticeably higher than in the previous cases. For the cases involving the SRRC shaping filter, the amplitude modulation induced by the filters requires more power in the orthogonal complement directions (compared to the RECT cases) to realize a set of constant amplitude waveforms.

Now consider the cross-correlation of the signal captured in the direction of each radar beam with the intended up-chirped LFM radar waveform. The SNR of the radar beam prior to filtering was determined to be 33.16 dB. For each case, the 20 pulses are captured in the direction of the radar beam and then Doppler processed (see Fig. 8). Each response resembles the typical range-Doppler point spread function of an LFM. For all four cases, the range sidelobes cohere at zero Doppler indicating that the sidelobe structures are consistent over the 20 pulses. The zero Doppler cut of each case is likewise shown in Fig. 9, where the sidelobe structure is nearly identical over the four cases and is very close to what is expected for the autocorrelation of an LFM waveform.

The signal emitted in the communication direction $\theta_c = 30°$ was captured and determined to have an average SNR of 21.13 dB (12.03 dB less than the radar signal, 0.97 dB different from the design specification of 13 dB). For each case the communication signal was demodulated using a

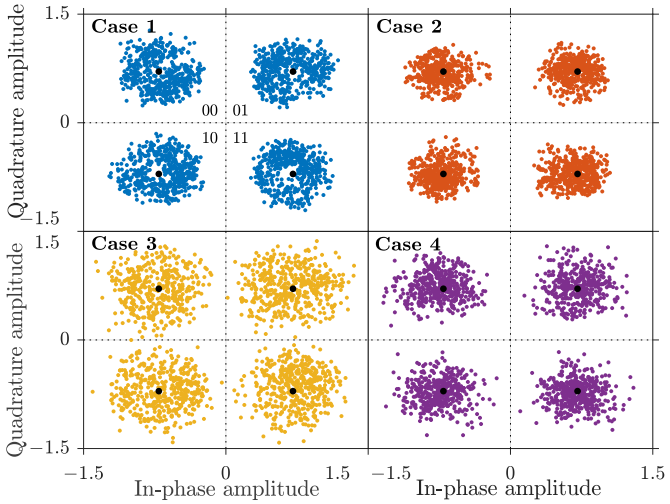

Fig. 10. Constellation scatter plot for case 1 (blue), case 2 (red), case 3 (yellow), and case 4 (purple).

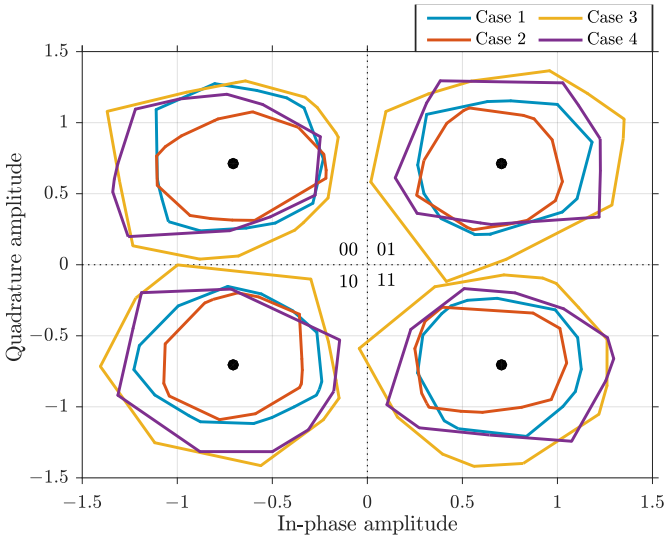

Fig. 11. Convex hull of demodulated symbols with associated constellation symbol for case 1 (blue), case 2 (red), case 3 (yellow), and case 4 (purple).

Maximum-Likelihood estimator [14] and compared against the known bit sequence that was transmitted. Recall that cases 1 and 2 involved a total of 4000 bits while cases 3 and 4 involved 3600 bits. For cases 1, 2, and 4, zero bit errors were found, while 2 bit errors occurred for case 3.

A communication scatter plot for each case is shown in Fig. 10. Note that case 2 (RECT shaping filter; $\theta_r = 0°$) produced the tightest grouping while case 3 produced the broadest grouping. A tighter grouping is associated with a better estimate of the true symbol value.

The convex hull of the demodulated symbols with the associated true constellation value for each is depicted in Fig. 11. Note that the two bit errors for case 3 (yellow) are discernible in the '01' and '11' quadrants. It is also observed that the groupings for the RECT cases (1-blue and 2-red) are more consistent than the SRRC cases (3-yellow and 4-purple). This result is likely due to the communication signal in cases 3 and 4 being more sensitive to transmit model errors due to the resulting amplitude modulation from the SRRC shaping filter. Also, the groupings for the cases having radar direction $\theta_r = -15°$ (1-blue and 3-yellow) cover a larger area than the cases having radar direction $\theta_r = 0°$ (2-red and 4-purple). The disparity between these results indicates that the transmit model (steering vector) used for the radar direction $\theta_r = 0°$ better approximates the actual transmitter effects.

It is also interesting to examine the structure of the fast-time signal in other spatial directions. Specifically, consider the impact of applying the communication ML estimator [14] to the signal captured from different directions. Comparing the results to the known bit sequences (and phase rotating as needed to assess the minimum possible bit error) as a function of angle produces the angle-dependent measured bit error rates (BER) shown in Fig. 12 for the four test cases. In the intended communication direction of $\theta_c = 30°$ the previous good results are observed: for cases 1, 2 and 4 have no bit errors (BER $= 0$) while case 3 yields BER $= 5.5 \times 10^{-4}$

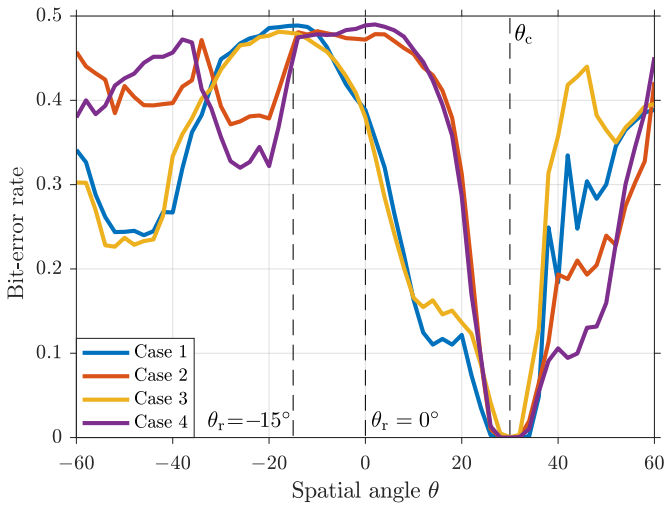

Fig. 12. Bit-error rate versus spatial angle for case 1 (blue), case 2 (red), case 3 (yellow), and case 4 (purple).

(2 errors out of 3600 bits). However, for other spatial angles, the BER increases significantly because the fast-time signals in those directions does not possess the expected communication signal structure. Note that the worst possible BER is 0.5 which is the expected value of BER for truly random bit estimates. The BER plots are shown in a linear scale instead of the traditional logarithmic scale as the curve shows more detail in angles away from the communications direction and to prevent the plots at $\theta = 30°$ from decreasing to minus infinity. Note cases possessing the same radar/communication spatial separation (cases 1 and 3 for $\theta_r = 15°$ and cases 2 and 4 for $\theta_r = 0°$) also realize similar BER responses. The "dips" at $\theta = -50°$ (cases 1 and 3) and $\theta = -25°$ (cases 2 and 4) could be a result of multipath as the tests were not administered in an anechoic chamber.

IV. Conclusion

The FFRED formulation, theoretically derived in the companion paper to produce a set of MIMO waveforms that realize simultaneous radar and communication emissions in the far-field, was here demonstrated experimentally in hardware. It was shown using a four-channel SDR testbed that constant amplitude, spectrally well-contained waveforms can be designed such that their measured emissions match quite well with the expected radar waveform in one direction and a readily demodulated communication signal in another direction. It was likewise observed that the signal emitted in other spatial directions does not retain the expected communication signal structure, thereby yielding a form of direction-dependent communications.

Acknowledgment

This work was supported by a subcontract with Matrix Research, Inc. for research sponsored by AFRL under Prime Contract # FA8650-14-D-1722.

References

[1] G. C. Tavik, C. L. Hilterbrick, J. B. Evins, J. J. Alter, J. G. Crnkovich, J. W. de Graaf, W. Habicht, G. P. Hrin, S. A. Lessin, D. C. Wu, and S. M. Hagewood, "The advanced multifunction RF concept," *IEEE Trans. Microw. Theory Tech.*, vol. 53, no. 3, pp. 1009–1020, March 2005.

[2] P. M. McCormick, S. D. Blunt, and J. G. Metcalf, "Simultaneous radar and communications emission from a common aperture, Part I: Theory," in *2017 IEEE Radar Conference*, May 2017.

[3] B. Friedlander, "On transmit beamforming for MIMO radar," *IEEE Trans. Aerosp. Electron. Syst.*, vol. 48, no. 4, pp. 3376–3388, October 2012.

[4] D. R. Fuhrmann and G. S. Antonio, "Transmit beamforming for MIMO radar systems using signal cross-correlation," *IEEE Trans. Aerosp. Electron. Syst.*, vol. 44, no. 1, pp. 171–186, January 2008.

[5] H. He, P. Stoica, and J. Li, "Wideband MIMO systems: Signal design for transmit beampattern synthesis," *IEEE Trans. Signal Process.*, vol. 59, no. 2, pp. 618–628, Feb 2011.

[6] O. Aldayel, V. Monga, and M. Rangaswamy, "Tractable MIMO beampattern design under constant modulus waveform constraint," in *2016 IEEE Radar Conference*, May 2016, pp. 1–6.

[7] P. M. McCormick, S. D. Blunt, and J. G. Metcalf, "Wideband MIMO frequency modulated emission design with space-frequency nulling," *IEEE J. Sel. Topics Signal Process.*, vol. 11, no. 2, pp. 363–378, March 2017.

[8] S. D. Blunt and E. L. Mokole, "Overview of radar waveform diversity," *IEEE Aerosp. Electron. Syst. Mag.*, vol. 31, no. 11, pp. 2–42, November 2016.

[9] A. Levi and H. Stark, "Image restoration by the method of generalized projections with application to restoration from magnitude," in *Acoustics, Speech, and Signal Processing, IEEE International Conference on ICASSP '84.*, vol. 9, Mar 1984, pp. 88–91.

[10] H. H. Bauschke, P. L. Combettes, and D. R. Luke, "Phase retrieval, error reduction algorithm, and fienup variants: a view from convex optimization," *JOSA A*, vol. 19, no. 7, pp. 1334–1345, 2002.

[11] L. K. Patton and B. D. Rigling, "Phase retrieval for radar waveform optimization," *IEEE Trans. Aerosp. Electron. Syst.*, vol. 48, no. 4, pp. 3287–3302, October 2012.

[12] J. R. Fienup, "Phase retrieval algorithms: a comparison," *Applied optics*, vol. 21, no. 15, pp. 2758–2769, 1982.

[13] T. C. Mealey and A. J. Duly, "BEEMER: A firmware-tuned, software-defined MIMO radar testbed," in *2016 IEEE International Symposium on Phased Array Systems and Technology (PAST)*, Oct 2016, pp. 1–6.

[14] J. G. Proakis, "Digital communications," *McGraw-Hill, New York, 5th ed.*, 2008.